PHYSICAL REVIEW E **92**, 011101(R) (2015)

Role of the ionization potential in nonequilibrium metals driven to absorption saturation

R. Mincigrucci,[1,2,*] F. Bencivenga,[1] F. Capotondi,[1] E. Principi,[1] E. Giangrisostomi,[1,3]
A. Battistoni,[1,3] M. Caputo,[1] F. Casolari,[1] A. Gessini,[1] M. Manfredda,[1] E. Pedersoli,[1] and C. Masciovecchio[1,†]
[1]*Elettra-Sincrotrone Trieste, SS 14-km 163.5, 34149 Basovizza, Trieste, Italy*
[2]*Dipartimento di Fisica e Geologia, Università degli Studi di Perugia, Via A. Pascoli, 06123 Perugia, Italy*
[3]*Dipartimento di Fisica, Università degli Studi di Trieste, via A. Valerio 2, 34127 Trieste, Italy*
(Received 26 March 2015; published 31 July 2015)

A composite metallic foil (Al/Mg/Al) has been exposed to intense sub-100 fs free electron laser (FEL) pulses and driven to ultrafast massive photoionization. The resulting nonequilibrium state of matter has been monitored through absorption spectroscopy across the $L_{2,3}$ edge of Mg as a function of the FEL fluence. The raw spectroscopic data indicate that at about 100 J/cm^2 the main absorption channels of the sample, i.e., Mg ($2p \rightarrow$ free) and oxidized Al (valence $\rightarrow$ free), are almost saturated. The spectral behavior of the induced transparency has been interpreted with an analytical approach based on an effective ionization potential of the generated solid-density plasma.

DOI: 10.1103/PhysRevE.92.011101 PACS number(s): 52.25.Jm, 41.60.Cr, 78.47.J−

It has been recently observed that core-level photoabsorption channels in metals can be saturated by ultrashort high-energy density extreme ultraviolet (EUV) or x-ray pulses, leading to transient transparency [1–7]. In the EUV case, the drastic opacity drop can be assigned to an excess of core holes in the probed sample volume and the subsequent reduction of atomic sites available for photoabsorption. This occurs because the photoionization rate exceeds the Auger recombination rate upon the interaction of the laser pulse with the specimen. A further consequence of the massive photoionization is the ultrafast heating of the valence electron system resulting from the scattering of photoelectrons [8]. Consequently, the absorption saturation process is accompanied by a sudden isochoric heating of the electron system over a cold solid-density ion lattice. This exotic state of matter can be described as a nonequilibrium dense plasma, whose physical properties are mostly unknown and scarcely predictable [9].

Under these nonequilibrium conditions the thermodynamic properties, the equations of state, as well as the opacity of the excited system are expected to be directly related to the ionization potential ($\mathcal{E}$) [10,11]. For this reason, the knowledge of this physical quantity in materials driven to nonequilibrium conditions represents a crucial step toward the control of physical properties in laser-excited matter, with significant benefits both in fundamental physics [12] and in technologies, such as inertial confinement fusion [13,14].

However, $\mathcal{E}$ is not invariant under high-ionization conditions, such as those induced by high-energy density EUV lasers on solid targets. Specific theoretical tools are demanded to evaluate $\mathcal{E}$ in this regime [11]. It is well known that the increase of the free electron density in an equilibrium plasma intensifies the electrical microfield resulting from the reciprocal electrostatic interaction between charged particles [15]. This effect induces an ionization potential depression (IPD). Emission spectroscopy measurements in a solid-density Al plasma [10] excited by an x-ray free electron laser (FEL), corroborated by tailored density functional theory (DFT) calculations [11,16], indicate that standard semiclassical methods underestimate the IPD effect in nonequilibrium solid-density plasmas. These findings stimulate further efforts to better comprehend the origin of the $\mathcal{E}$ variation in nonequilibrium solid materials, as well as to contrive new experimental techniques suitable to provide a direct measurement of that essential physical quantity. An alternative approach to determine the $\mathcal{E}$ changes is to model their effect on the material absorption coefficient [4]. Indeed, as quoted above, the drastic attenuation of the absorption cross section is ineluctably related to the creation of a uniform solid-density hot plasma accompanied by a transient alteration of the ionization balance.

In this Rapid Communication we explore this approach, presenting a unique campaign of saturation absorption measurements on aluminum-capped magnesium thin foils (Al/Mg/Al) as a function of both the FEL fluence (F) and photon energy ($h\nu$) across the Mg $L_{2,3}$ edge (∼50 eV). The experiment was carried out at the EIS-TIMEX end station [17] operative at the FERMI FEL in Trieste (Italy). FERMI is a tunable seeded FEL capable of delivering nearly transform-limited sub-100 fs pulses in the EUV–soft x-ray spectral region of $h\nu$ 300–20 eV [18]. The experimental setup consists of a gas ionization chamber (I0M) [19], monitoring the incoming FEL intensity (I_{in}), an ellipsoidal gold coated mirror (EFM) with a focal length of 1.4 m, and focusing the FEL beam down to 6 μm full width at half maximum (FWHM) at the sample plane. The sample (LUXEL, USA) consists of a central layer of Mg (140 nm thick) protected on both sides with an Al coating (20 nm nominal thickness); see Fig. 1. The thickness of the oxidized fraction in the Al layers was evaluated on a similar sample to be about 7 nm through x-ray photoemission spectroscopy (XPS) combined with argon sputtering; this procedure is described in the Supplemental Material [20].

The transmitted intensity (T) was measured by a UVG20C photodiode (PHD) by Opto Diode, coupled to a 100 nm Al-coated, Ce-doped YtAl garnet (YAG:Ce) screen. The Al coating serves to screen the YAG optical transducer from the residual seed laser radiation (295–320 nm) copropagating

*riccardo.mincigrucci@elettra.eu
†claudio.masciovecchio@elettra.eu

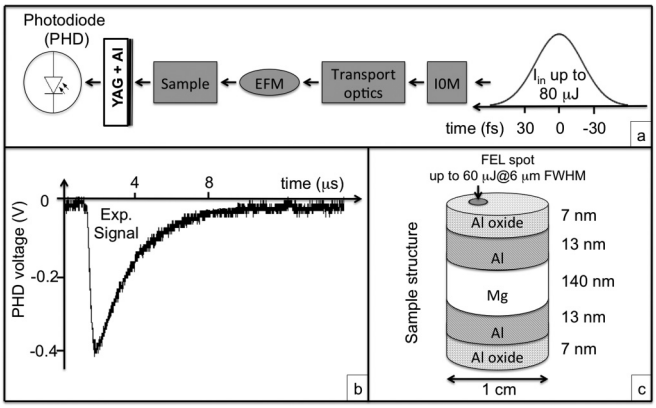

FIG. 1. (a) Sketch of the experimental setup with the Al/Mg/Al sample normal to the FEL beam. I_{in} was measured using a gas ionization chamber (I0M) while the transmitted signal was recorded through a UVG20C photodiode (PHD) coupled to a YAG screen. The beam line transmission [transport and focusing (EFM) optics] is estimated to be $T = 0.76$ in the probed $h\nu$ range (47.7–52.9 eV). (b) Typical experimental signal measured by the photodiode. (c) Sketch of the sample structure.

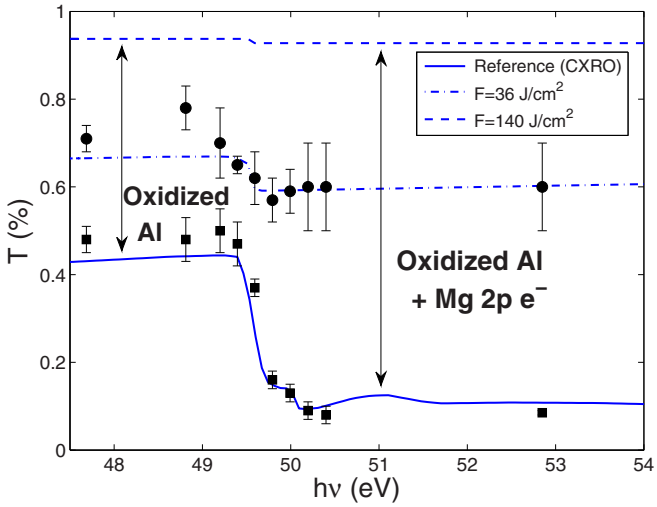

FIG. 2. (Color online) Comparison of experimental low-F (squares) and high-F (circles) data with theoretical curves. Low-F data are compared with the T spectrum of the sample stack described in Fig. 1 at ambient conditions (solid curve) [22]. Dashed-dotted and dashed curves are the sample transmission at fluences of 36 and 140 J/cm^2, respectively, calculated by the analytical model discussed in the text.

with the FEL pulse. Data from the PHD and I0M were collected shot by shot by a real time acquisition infrastructure [21]. Measurements were carried out within the $h\nu$ 47.7–52.9 eV spectral window. For each $h\nu$ value, a calibration curve has been recorded as a function of I_{in}. Moreover, for each photon energy, a set of low-F T measurements were performed at $F = 0.02$ J/cm^2 i.e., 20 times smaller than the measured damage threshold ($F_d = 0.4$ J/cm^2), in order to determine a reference T spectrum for the sample at equilibrium ambient conditions. High-F measurements were performed in a single-shot fashion, automatically moving the sample to a nonirradiated position prior to a subsequent exposure. Figure 2 reports the comparison between theoretical (Ref. [22], solid line) and experimental (squares) low-F spectral transmission of the sample. The error bars for these measurements result from the standard deviations of 500 points. High-F spectral transmission predicted by the analytical model discussed below for $F = 36$ and 140 J/cm^2 are reported and compared to experimental data collected at $F = 36$ J/cm^2. The theoretical transmissions under ambient conditions for the different layers composing the sample are $T \sim 55\%$ for 14 nm of Al oxide, $T \sim 95\%$ for 26 nm of Al, and $T \sim 90\%$ and 20% for 140 nm of Mg before and after the $L_{2,3}$ edge, respectively. The spectroscopic results shown in Fig. 2 reflect those values and points out that the absorption in the investigated spectral region is mainly ascribed to the Mg $2p \rightarrow$ free (for $h\nu > 49.5$ eV) and Al oxide valence $\rightarrow$ free channels.

When exposed to a fluence of 36 J/cm^2, the sample exhibits a radical increase in T both before and after the $L_{2,3}$ edge of Mg, accompanied by an evident attenuation of the absorption jump at the edge. These effects indicate that both the principal absorption channels of the sample are subject to pronounced saturation. Above 140 J/cm^2 both channels are expected to be completely saturated as the overall transmission of the sample is estimated to be about $T = 95\%$ in the whole spectral range under investigation. Figure 3 displays the experimental values of transmission T as a function of fluence F for different $h\nu$ values across the Mg $L_{2,3}$ edge. Each point is a binning on F (4 J/cm^2 bin size); errors bars are one standard deviation. The FEL pulse duration was estimated to be 65 fs (12th harmonics of the seed laser with a time duration of 147 fs [23]) which is comparable to the core-hole lifetime of Mg, expected to be in the 15–65 fs range [24,25]. Experimental data in Fig. 3 have been modeled by using an analytical approach based on a classical approximation [26], which postulates a linear dependence of the absorption coefficient (μ^i) on the energy density ϵ (here expressed in eV/particle) deposited in the sample volume exposed to the FEL radiation,

$$\mu_i(F,t) = \mu_i^0\left(1 - \frac{\epsilon_i(F,t)}{\widetilde{\mathcal{E}}_i}\right), \qquad (1)$$

where the layer index i runs from 1 to 5, according to the sample structure shown in Fig. 1, $\widetilde{\mathcal{E}}_i$ is the effective ionization potential of the ith layer, and the dependence of μ_i and μ_i^0 on $h\nu$ is tacit. Equation (1) reflects what is experimentally observed, namely, that the decrease in μ_i occurs at high ϵ_i values, i.e., at high F. The level of ionization resulting from the deposition of the pulse energy depends on the effective ionization potential $\widetilde{\mathcal{E}}_i$ of the excited system that appears in the denominator of Eq. (1). Systems with large $\widetilde{\mathcal{E}}$ are then expected to be less inclined to absorption saturation. The advantage of using a photon energy (about 50 eV) comparable to the ionization energy of Mg is that multi-ionization processes are unlikely, thus allowing us to treat $\widetilde{\mathcal{E}}_3$ as the value of the first ionization potential. For simplicity, we extend this assumption to the Al and oxidized Al layers, which implies that each unexcited particle in a given layer (Fig. 1) linearly contributes to the absorption, while the excited ones do not contribute at all. Therefore, at a certain time (t), the energy density deposited

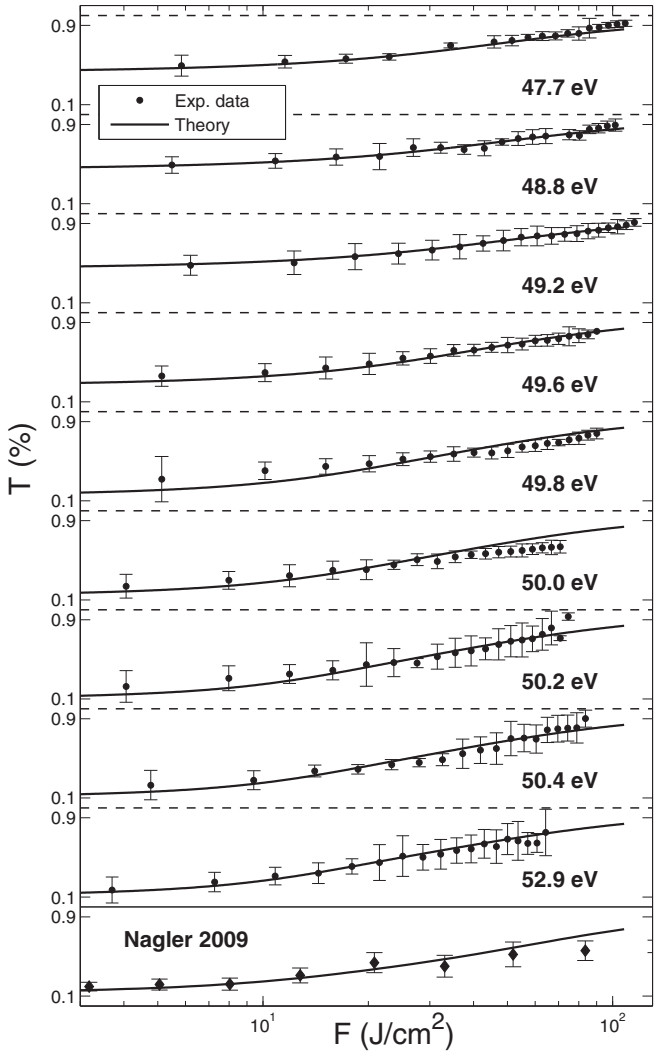

FIG. 3. Experimental values of $T(F)$ as a function of F across the magnesium $L_{2,3}$ edge and corresponding theoretical curves predicted by the model described in the text. In the lowest part, a comparison of data from Ref. [1] (diamond) is shown against a model prediction for aluminum in the same fluence interval of our experiment.

onto a sample layer i can be written as

$$\epsilon_i(F,t) = \frac{E_i^d(F,t)}{N_i} = \frac{1}{N_i}\int_{-\infty}^{t}(1-e^{-\mu_i(F,t')s_i})G_i(t')dt', \tag{2}$$

where, assuming a negligible EUV reflectivity of the sample, E_i^d is the amount of energy deposited in the ith layer of thickness s_i, N_i is the number of particles in the ith layer exposed to the FEL, and G_i is recursively defined as

$$G_i(t') = \begin{cases} g(t'), & i=1, \\ e^{-\mu_{i-1}(F,t')s_i}G_{i-1}(t'), & i=2,\ldots,5, \end{cases} \tag{3}$$

where $g(t')$ is a Gaussian profile of 65 fs FWHM, resembling typical pulses delivered by FERMI [31], with a total area equal to I_{in}. The effective ionization potential for the Mg layer ($i=3$) has been modeled as

$$\widetilde{\mathcal{E}}_3 = \frac{\mathcal{E}_3}{1-\Theta\left(E_3^e-h\nu\right)A_3}, \tag{4}$$

where $\mathcal{E}_3$ is the ionization potential for room temperature solid Mg, and Θ is the Heaviside function mimicking the steep absorption change at the edge ($E_3^e = 50$ eV).

A_3 is a free parameter in the model that accounts for the ionization energy difference between solid Mg at room temperature and the nonequilibrium solid-density Mg plasma probed in the present work. The Al and Al oxide layers are well described by a single value of $\widetilde{\mathcal{E}}_i$ for the whole spectral window as they do not exhibit any core-level absorption edge in that $h\nu$ range. For Al we have assumed $\widetilde{\mathcal{E}} = 53.31$ eV, according to Ref. [27], while for the oxidized Al we fitted the value of $\widetilde{\mathcal{E}}_{1,5}$ being below the absorption L_1 edge of oxygen. The oxidized layer is a nonstochiometric oxide, so we approximated it as a mixture of Al and O atoms in a ratio determined by the XPS measurements. This enabled us to define the number of moles of oxide particles in the excited volume as the ratio between the effective oxide molar volume and the volume exposed to the FEL. We found that the average $N^{\text{O}}/N^{\text{Al}}$ ratio, where N^{O} and N^{Al} are the number density of oxygen and aluminum atoms, is about 3, so that every virtual particle of oxidized Al contains three oxygen atoms. This is in accordance with the oxidation theory of metals which predicts a gradual oxygen concentration decrease as a function of the depth from the surface [32].

$T(F)$ is finally calculated as the total transmitted intensity divided by I_{in}, i.e.,

$$T(F,h\nu) = \frac{\int_{-\infty}^{\infty}\prod_{i=1}^{5}e^{-\mu_i(F,t)s_i}g(t)dt}{I_{\text{in}}}. \tag{5}$$

We point out that the absorption channels involved in the investigated process exhibit a recombination time longer than the FEL pulse duration. Therefore, the measured transmission increase results from a cumulative process dependent on the time distribution function $g(t')$ [see Eqs. (2) and (3) and the Supplemental Material]. The whole set of experimental transmission data as a function of F and $h\nu$ has been fitted using a genetic algorithm based on Eqs. (1)–(5) (solid curves in Fig. 3), in which the $\widetilde{\mathcal{E}}_{1,5}$ and A_3 parameters were left free to vary. Best fit values for the free parameters of the algorithm are $\widetilde{\mathcal{E}}_{1,5} = 270 \pm 10$ eV/particle and $\widetilde{\mathcal{E}}_3 = 42 \pm 2$ eV/particle for $h\nu > E_3^e$ (with $A_3 = 0.46 \pm 0.03$). Interestingly, this value well compares with that of 44 eV for the $Mg^{2+} \rightarrow Mg^{3+}$ ionization in the Mg plasma, as predicted by common theoretical models for classical plasmas [15,28] (Table I). This model has been found to be consistent also with the experimental results obtained by Ciricosta *et al.* for Al [10]. The value obtained for $\widetilde{\mathcal{E}}_{1,5}$ is compatible with the energy required to extract six $2s$ electrons (those available in the oxygen atoms present in a virtual Al oxide particle) from the lower valence band of alumina [33]. The saturation of this absorption channel is associated with the dramatic opacity attenuation in the spectral region before the Mg $L_{2,3}$ edge (see Fig. 2). The best fit curves calculated by our model have been compared with standard rate equation curves, exhibiting a better agreement with the experimental data (see the Supplemental Material).

The quantity $1-A$ calculated by the model [the denominator in Eq. (4)] effectively describes how much the ionization potential of a certain material (Mg, in our case) is altered by the massive ionization induced by the bound-free

TABLE I. $\mathcal{E}$ values for Mg, Al, and oxidized Al. The columns reports, from left to right, the calculated value for the solid at room conditions, the Ecker-Kröll and Stewart-Pyatt predictions for dense equilibrium plasma, the values obtained by our model ($\widetilde{\mathcal{E}}$) for solid-density nonequilibrium plasma, and the value for an isolated ion.

Process	Solid: Room conditions ($\mathcal{E}$) (eV/particle)	Dense equil. plasma (eV/particle)	Solid-density nonequil. plasma ($\widetilde{\mathcal{E}}$) (eV/particle)	Isolated ion (eV/particle)
$Mg^{2+} \rightarrow Mg^{3+}$	22.67[a]	44,[b] 43[c]	42 ± 2	80[d]
$Al^{3+} \rightarrow Al^{4+}$	53.31[a]	62,[b] 66[c]	64 ± 3	120[d]
Oxid. Al valence $\rightarrow$ free			270 ± 10	

[a]Reference [27].
[b]Reference [15].
[c]Reference [28].
[d]References [29,30].

absorption process. According to both Ecker-Kröll (EK) [15] and Stewart-Pyatt (SP) [28] models, the IPD effect is related to the charge density and thus ultimately to the atomic density. Therefore, the factor $1 - A$ is likely to be material dependent and to linearly scale with the atomic density. This allows us, for example, to estimate $1 - A$ for Al using the value obtained by our fit for Mg, $(1 - A_{2,4}) = (1 - A_3)\frac{\rho_{Al}}{\rho_{Mg}}$. Following this assumption, the expected value of $A_{2,4}$ for Al is 0.16 ± 0.03. This value, combined with the first ionization energy of solid Al (53.31 eV/particle [27]), yields $\widetilde{\mathcal{E}}_{2,4} = 64 \pm 3$ eV/particle for the $Al^{3+} \rightarrow Al^{4+}$ process in the solid-density plasma regime. Such a value well compares with the ionization energy of the Al plasma, recently determined as 67 ± 7 eV/particle [10], as well as with EK and SP classical plasma predictions [15,28] (Table I). Using this value for the effective ionization potential for Al, the proposed model is able to well reproduce the saturable absorption experiment carried out by Nagler *et al.* [1] (bottom of Fig. 3), where the saturation process of oxidized Al layers, assumed to be 7 nm thick, on both sides of the sample has been considered.

In conclusion, we have shown a unique experimental study on induced transient transparency on a composite metallic sample (Al/Mg/Al) driven by FEL exposure in an extended EUV spectral region. The spectroscopy of the saturable absorption process allowed us to distinguish between two main absorption channels by tuning the FEL photon energy across the $L_{2,3}$ edge of Mg. The first one is related to $2p$ electron absorption in Mg, similar to that already observed in Al [1]. The second is most likely related to oxygen $2s$ electrons.

An analytical approach has been proposed, based on the assumption that the ionization potential in the FEL-driven solid-density plasma plays a crucial role in the opacity attenuation process. That approach has been found to precisely model the experimental data as well as to provide a realistic estimation of the effective ionization potential for nonequilibrium solid-density Mg. The proposed model has been also successfully applied to previous saturable absorption data for Al [1], giving an estimation of the ionization potential for nonequilibrium dense Al that is in agreement with recent experimental findings [10]. These results stimulate a further development of the method aimed at improving its predictive capabilities and extending its application to further experimental cases. Future advances should regard the investigation of absorption saturation under higher ionization states, thus providing a sensitive tool to test the validity of available EK and SP models in nonequilibrium solid-density plasmas.

The authors acknowledge useful discussions with S. Vinko. A critical reading of the manuscript by R. Cucini, M. G. Izzo, and M. Kiskinova is acknowledged. XPS measurements were carried in collaboration with A. Goldoni. Excellent technical support from the PADReS group is reported.

[1] B. Nagler, U. Zastrau, R. Fäustlin *et al.*, Nat. Phys. **5**, 693 (2009).
[2] H. Yoneda, Y. Inubushi, T. Tanaka *et al.*, Opt. Express **17**, 23443 (2009).
[3] H. Yoneda, Y. Inubushi, M. Yabashi, T. Katayama, T. Ishikawa, H. Ohashi, H. Yumoto, K. Yamauchi, H. Mimura, and H. Kitamura, Nat. Commun. **5**, 5080 (2014).
[4] D. S. Rackstraw, O. Ciricosta, S. M. Vinko *et al.*, Phys. Rev. Lett. **114**, 015003 (2015).
[5] L. Young, E. P. Kanter, B. Krässig *et al.*, Nature (London) **466**, 56 (2010).
[6] M. Hoener, L. Fang, O. Kornilov *et al.*, Phys. Rev. Lett. **104**, 253002 (2010).
[7] S. Schorb, D. Rupp, M. L. Swiggers *et al.*, Phys. Rev. Lett. **108**, 233401 (2012).
[8] B. Rethfeld, A. Kaiser, M. Vicanek, and G. Simon, Phys. Rev. B **65**, 214303 (2002).
[9] *Frontiers and Challenges in Warm Dense Matter*, edited by F. Graziani, M. Desjarlais, R. Redmer, and S. Trickey, Lecture Notes in Computational Science and Engineering Vol. 96 (Springer, Berlin, 2014).
[10] O. Ciricosta, S. M. Vinko, H.-K. Chung *et al.*, Phys. Rev. Lett. **109**, 065002 (2012).
[11] S. M. Vinko, O. Ciricosta, and J. S. Wark, Nat. Commun. **5**, 3533 (2014).
[12] M. Beye, S. Schreck, F. Sorgenfrei, C. Trabant, N. Pontius, C. Schüßler-Langeheine, W. Wurth, and A. Föhlisch, Nature (London) **501**, 191 (2013).
[13] J. D. Lindl, P. Amendt, R. L. Berger, S. G. Glendinning, S. H. Glenzer, S. W. Haan, R. L. Kauffman, O. L. Landen, and L. J. Suter, Phys. Plasmas **11**, 339 (2004).
[14] L. B. Fletcher, A. L. Kritcher, A. Pak *et al.*, Phys. Rev. Lett. **112**, 145004 (2014).

[15] G. Ecker and W. Kröll, Phys. Fluids **6**, 62 (1963).
[16] S.-K. Son, R. Thiele, Z. Jurek, B. Ziaja, and R. Santra, Phys. Rev. X **4**, 031004 (2014).
[17] C. Masciovecchio, A. Battistoni, E. Giangrisostomi *et al.*, J. Synchrotron Radiat. **22**, 553 (2015).
[18] E. Allaria, A. Battistoni, F. Bencivenga *et al.*, New J. Phys. **14**, 113009 (2012).
[19] M. Zangrando, A. Abrami, D. Bacescu *et al.*, Rev. Sci. Instrum. **80**, 113110 (2009)
[20] See Supplemental Material at http://link.aps.org/supplemental/10.1103/PhysRevE.92.011101 for a brief description of the XPS measurement, a second data set, a comparison of our model with standard rate equations, and a demonstration of the model sensitivity to the used parameters.
[21] R. Borghes, V. Chenda, A. Curri, G. Kourousias, M. Lonza, M. Prica, R. Pugliese, and G. Passos, A common software framework for FEL data acquisition and experiment management at FERMI, in *Proceedings of the 14th International Conference on Accelerator and Large Experimental Physics Control Systems, San Francisco, California, USA* (JACoW, 2013), pp. 1481–1484, http://jacow.org/.
[22] B. Henke, E. Gullikson, and J. Davis, At. Data Nucl. Data Tables **54**, 181 (1993).
[23] D. Ratner, A. Fry, G. Stupakov, and W. White, Phys. Rev. ST Accel. Beams **15**, 030702 (2012).
[24] C.-O. Almbladh, A. L. Morales, and G. Grossmann, Phys. Rev. B **39**, 3489 (1989).
[25] M. Ohno and G. Van Riessen, J. Electron Spectrosc. **128**, 1 (2003).
[26] F. Bencivenga, E. Principi, E. Giangrisostomi *et al.*, Sci. Rep. **4**, 4952 (2014).
[27] H. Gupta, *Solid State Physics* (Vikas, Noida, 2001).
[28] J. C. Stewart and K. D. Pyatt, Astrophys. J. **144**, 1203 (1966).
[29] J. Huheey, *Inorganic Chemistry: Principles of Structure and Reactivity* (Harper & Row, New York, 1972).
[30] A. James and M. Lord, *MacMillan's Chemical and Physical Data* (MacMillan, London, 1992).
[31] E. Allaria, R. Appio, L. Badano *et al.*, Nat. Photonics **6**, 699 (2012).
[32] N. Cabrera and N. Mott, Rep. Prog. Phys. **12**, 163 (1949).
[33] S. Ciraci and I. P. Batra, Phys. Rev. B **28**, 982 (1983).